Inorg. Chem. **2006**, *45*, 6323–6330

Water Induces a Structural Conversion and Accelerates the Oxygenation of Carboxylate-Bridged Non-Heme Diiron Enzyme Synthetic Analogues

Min Zhao, Datong Song, and Stephen J. Lippard*

Department of Chemistry, Massachusetts Institute of Technology, Cambridge, Massachusetts 02139

Received February 20, 2006

Recently, we reported the synthesis of a carboxylate-rich non-heme diiron enzyme model compound $[Fe_2(\mu\text{-}O_2CAr^{Tol})_4(4\text{-}CNPy)_2]$ (**1**), where $^{-}O_2CAr^{Tol}$ is 2,6-di-*p*-tolylbenzoate and 4-CNPy is 4-cyanopyridine (Yoon, S.; Lippard, S. J. *J. Am. Chem. Soc.* **2005**, *127*, 8386–8397). A metal-to-ligand charge-transfer band in the visible region of the optical absorption spectrum involving the nitrogen-donor ligand endowed this complex with a distinctive red color that facilitated analysis of its chemistry. Following this strategy, we prepared and characterized two related isomeric complexes, windmill (**3**) and paddlewheel (**4**) species having the formula $[Fe_2(O_2CAr^{Tol})_4(4\text{-}AcPy)_2]$, where 4-AcPy is 4-acetylpyridine. In anhydrous solvents, **1** and **4** adopt paddlewheel structures, but upon the addition of water, they convert to aquated forms, windmill structures having the composition $[Fe_2(\mu\text{-}O_2CAr^{Tol})_2(O_2CAr^{Tol})_2(4\text{-}RPy)_2(H_2O)_2]$. This conversion is favored at low temperature and was studied by NMR spectroscopy. A kinetic analysis of the aquation reaction was undertaken by stopped-flow measurements between 198 and 223 K for both **1** and **4**, which revealed a first-order dependence on both the diiron compound and water. The oxygenation rates for the water-containing complexes are much faster than those for the corresponding anhydrous complexes, being 20-fold faster for **4** and 10-fold more rapid for **1**. The presence or absence of water had little effect on the activation enthalpies, suggesting that the loss of water may not be necessary prior to dioxygen binding in the transition state.

Introduction

Metalloproteins play important roles in living cells. Non-heme diiron enzymes including soluble methane monooxygenase (sMMO),[1−3] the R2 subunit of ribonucleotide reductase (RNR-R2),[4] fatty acid desaturase (Δ^9D),[5,6] and toluene/*o*-xylene monooxygenase[7,8] activate dioxygen to perform a variety of functions. Their active-site structures share a common feature, two bridging carboxylates that support coordinatively unsaturated diiron centers, each having an additional terminal carboxylate and a histidine ligand.[6,7,9−11] The nature of the diiron cores in these enzymes differs slightly as a consequence of the carboxylate binding modes and a variable number of water molecules. Understanding how these structurally related enzymes achieve different functions is a challenging current goal. The role of water in catalysis is difficult to discern in the aqueous environment of an enzyme. Thus far, such information has only been provided for soluble methane monooxygenase by computational analysis, from which it was concluded that water is important for the formation of intermediates in the catalytic cycle.[12]

We have begun to address the effects of water on the geometry and reactivity of carboxylate-bridged diiron centers by using synthetic model compounds. Previously, we dem-

* To whom correspondence should be addressed. E-mail: lippard@mit.edu.

(1) Feig, A. L.; Lippard, S. J. *Chem. Rev.* **1994**, *94*, 759−805.
(2) Wallar, B. J.; Lipscomb, J. D. *Chem. Rev.* **1996**, *96*, 2625−2657.
(3) Merkx, M.; Kopp, D. A.; Sazinsky, M. H.; Blazyk, J. L.; Müller, J.; Lippard, S. J. *Angew. Chem., Int. Ed.* **2001**, *40*, 2782−2807.
(4) Stubbe, J. A.; van der Donk, W. A. *Chem. Rev.* **1998**, *98*, 2661−2661.
(5) Shanklin, J.; Whittle, E.; Fox, B. G. *Biochemistry* **1994**, *33*, 12787−12794.
(6) Lindqvist, Y.; Huang, W. J.; Schneider, G.; Shanklin, J. *EMBO J.* **1996**, *15*, 4081−4092.
(7) Sazinsky, M. H.; Bard, J.; Di Donato, A.; Lippard, S. J. *J. Biol. Chem.* **2004**, *279*, 30600−30610.
(8) Pikus, J. D.; Studts, J. M.; Achim, C.; Kauffmann, K. E.; Münck, E.; Steffan, R. J.; McClay, K.; Fox, B. G. *Biochemistry* **1996**, *35*, 9106−9119.
(9) Logan, D. T.; Su, X.-D.; Aberg, A.; Regnström, K.; Hajdu, J.; Eklund, H.; Nordlund, P. *Structure* **1996**, *4*, 1053−1064.
(10) Rosenzweig, A. C.; Nordlund, P.; Takahara, P. M.; Frederick, C. A.; Lippard, S. J. *Chem. Biol.* **1995**, *2*, 409−418.
(11) Whittington, D. A.; Lippard, S. J. *J. Am. Chem. Soc.* **2001**, *123*, 827−838.
(12) Baik, M.-H.; Newcomb, M.; Friesner, R. A.; Lippard, S. J. *Chem. Rev.* **2003**, *103*, 2385−2419.

10.1021/ic0602906 CCC: $33.50
Published on Web 07/15/2006

onstrated that the coordination geometry of carboxylate-rich diiron complexes is affected by the presence of water molecules in the environment.[13] In particular, diiron(II) complexes react with water,[14] and a diiron(II) compound with μ-aqua and μ-hydroxo bridges was reported in which the redox potential is almost 1 V more positive than that of its di-μ-hydroxo analogue.[15] The presence of water only moderately affected the reaction rate of this complex with dioxygen, however.[15] By contrast, a quantitative kinetic study of the effect of water on the oxygenation of carboxylate-bridged diiron(II) complexes having 4-cyanopyridine (4-CNPy) as the nitrogen donors revealed a significant effect on the reaction rate.[16] The chemistry could be readily followed by a shift of a metal-to-ligand charge-transfer (MLCT) band present in the visible region of the spectrum. The reaction of dioxygen with the compound [$Fe_2(\mu$-O_2CAr^{Tol})$_4$(4-CNPy)$_2$] (**1**) was monitored kinetically with and without water being present.[16] From a preliminary analysis, it was concluded that water reacts with **1** much more rapidly than dioxygen, forming the aqua compound [$Fe_2(\mu$-O_2CAr^{Tol})$_2$(O_2CAr^{Tol})$_2$(4-CNPy)$_2$(H_2O)$_2$] (**2**). In **2**, an open coordination site was generated as a result of a rapidly exchanging water molecule and the oxygenation reactivity was increased compared to that of the anhydrous compound **1**.

Following the same synthetic strategy, we prepared diiron(II) compounds containing the related 4-acetylpyridine (4-AcPy) ligand in place of 4-CNPy to generate paddlewheel and windmill isomers that differ in color. The aquation and oxygenation of the paddlewheel compound **4** was studied kinetically, as reported herein. We also present the results of detailed double-mixing stopped-flow kinetic studies of the reaction of **1** with water and the subsequent interaction of the aqua species with dioxygen. A more detailed mechanism is revealed by the data than previously could be deduced. NMR spectroscopy was utilized to monitor directly the formation of the water adduct.

Experimental Section

General Considerations. All reagents were purchased from commercial sources and used as received. Solvents were saturated with nitrogen and purified by passage through activated Al_2O_3 columns under nitrogen. Air-sensitive manipulations were performed under nitrogen in an MBraun drybox. The compounds [$Fe_2(\mu$-O_2CAr^{Tol})$_2$(O_2CAr^{Tol})$_2$(THF)$_2$],[17] [$Fe_2(\mu$-O_2CAr^{Tol})$_4$(4-CNPy)$_2$] (**1**),[16] and [$Fe_2(\mu$-O_2CAr^{Tol})$_2$(4-CNPy)$_2$(O_2CAr^{Tol})$_2$(H_2O)$_2$] (**2**)[16] were prepared as previously reported, where $^-O_2CAr^{Tol}$ is 2,6-di-*p*-tolylbenzoate[18,19] and 4-CNPy is 4-cyanopyridine.

Physical Measurements. 1D ^{1}H NMR spectra were recorded on VARIAN Mercury 300 MHz and VARIAN Inova 500-MHz spectrometers, and a 2D COSY NMR spectrum was obtained with a VARIAN Inova 500-MHz spectrometer using CD_2Cl_2 as the solvent. Chemical shifts were referenced to deuterated solvent peaks. Fourier transform infrared (FT-IR) spectra were recorded on a Bio Rad FTS-135 instrument. UV−vis spectra were measured on a Hewlett-Packard 8453 diode array spectrophotometer.

[$Fe_2(\mu$-O_2CAr^{Tol})$_2$(O_2CAr^{Tol})$_2$(4-AcPy)$_2$] (3). To a rapidly stirred 4-mL CH_2Cl_2 solution of [$Fe_2(\mu$-O_2CAr^{Tol})$_2$(O_2CAr^{Tol})$_2$-(THF)$_2$] (174 mg, 119 μmol) was added 26.0 μL of 4-AcPy (238 μmol), and the yellow color instantly changed to red. Orange crystalline material (129 mg, 69.4%) was obtained by pentane vapor diffusion into the solution. FT-IR (KBr, cm^{-1}): 3051 (w), 2918 (w), 2864 (w), 1696 (m, $\nu_{C=O(acetyl)}$), 1605 (s), 1542 (m), 1515 (m), 1455 (m), 1420 (m), 1383 (s), 1362 (w), 1263 (m), 1227 (w), 1185 (w), 1109 (w), 1061 (w), 1031 (w), 857 (w), 844 (w), 817 (m), 801 (m), 791 (m), 780 (w), 766 (w), 735 (w), 712 (w), 595 (m), 546 (w), 526 (w), 454 (w), 406 (w). Anal. Calcd for $C_{98.75}H_{83.5}N_2O_{10}$-$Fe_2Cl_{1.5}$ (**3**·0.75CH_2Cl_2): C, 73.07; H, 5.19; N, 1.73. Found: C, 73.08; H, 4.76; N, 1.72.

[$Fe_2(\mu$-O_2CAr^{Tol})$_4$(4-AcPy)$_2$] (4). The compound was obtained as a red powder by dissolving **3** in CH_2Cl_2 and evaporating the solvent under reduced pressure. Plate-like crystals suitable for X-ray diffraction studies were grown together with needles of **3** from vapor diffusion of pentane into a concentrated solution in CH_2Cl_2. FT-IR (KBr, cm^{-1}): 3051 (w), 2918 (w), 2864 (w), 1697 (s, $\nu_{C=O(acetyl)}$), 1605 (s), 1552 (s), 1515 (s), 1453 (s), 1419 (m), 1382 (s), 1361 (s), 1264 (s), 1185 (w), 1147 (w), 1109 (w), 1061 (w), 1031 (w), 1020 (w), 856 (w), 818 (s), 801 (s), 766 (m), 736 (w), 712 (w), 638 (w), 593 (m), 545 (w), 525 (m), 456 (w). UV−vis (CH_2Cl_2) λ_{max}, nm (ϵ, M^{-1} cm^{-1}): 495 (1300). ^{1}H NMR (CD_2Cl_2) δ (ppm): 112 (4H), 30.0 (4H), 13.0 (8H), 6.9 (16H), 6.3 (16H), 2.5 (6H), 1.8 (24H), 1.4 (4H). Anal. Calcd for $C_{98}H_{84}N_2O_{11}Fe_2$ (**4**·H_2O): C, 74.62; H, 5.37; N, 1.78. Found: C, 74.64; H, 5,03; N, 1.67.

Stopped-Flow Kinetic Experiments. Ambient-pressure kinetic experiments were carried out by using a Canterbury stopped-flow SF-40 and MG-6000 rapid diode array system (Hi-Tech Scientific). Stainless steel flow lines and an argon-purged anaerobic attachment were employed to avoid moisture and preoxidization. The mixing cell temperature was maintained at ±0.1 K. All lines of the instrument were extensively washed with dioxygen-free anhydrous solvent before conducting experiments. Solutions of **1** and **3** in CH_2Cl_2 were prepared in a drybox and stored in a gastight syringe prior to loading into the stopped-flow apparatus. A saturated solution of dioxygen was prepared by bubbling the gas through CH_2Cl_2 for 20 min in a septum-sealed round-bottomed flask maintained at 293 K, and the concentration was taken as 5.8 mM before mixing.[20] A CH_2Cl_2 solution containing 2 mM water was prepared by dissolving 9 μL of water in 250 mL of CH_2Cl_2. Oxygenation after aquation of the diiron(II) complexes was studied in the double-mixing mode. The diiron(II) compound and water were combined at low temperature in the first mixing chamber, incubated for 2 s, a time sufficient for the reaction to be complete, and then combined with a solution of dioxygen at the same low temperature in the second mixing chamber.

X-ray Crystallographic Studies. Single crystals coated with Paratone-N oil were mounted on the tips of quartz fibers at room temperature and cooled to 173 K under a stream of cold nitrogen. Intensity data were collected on a Bruker APEX CCD diffractometer with graphite-monochromated Mo Kα radiation (λ = 0.710 73 Å) using the SMART software package. Data collection and reduction

(13) Yoon, S.; Lippard, S. J. *J. Am. Chem. Soc.* **2004**, *126*, 16692−16693.
(14) Yoon, S.; Kelly, A. E.; Lippard, S. J. *Polyhedron* **2004**, *23*, 2805−2812.
(15) Korendovych, I. V.; Kryatov, S. V.; Reiff, W. M.; Rybak-Akimova, E. V. *Inorg. Chem.* **2005**, *44*, 8656−8658.
(16) Yoon, S.; Lippard, S. J. *J. Am. Chem. Soc.* **2005**, *127*, 8386−8397.
(17) Lee, D.; Lippard, S. J. *Inorg. Chem.* **2002**, *41*, 2704−2719.
(18) Du, C.-J. F.; Hart, H.; Ng, K.-K. D. *J. Org. Chem.* **1986**, *51*, 3162−3165.
(19) Chen, C.-T.; Siegel, J. S. *J. Am. Chem. Soc.* **1994**, *116*, 5959−5960.
(20) Battino, R. *Oxygen and Ozone*, 1st ed.; Pergamon Press: Oxford, U.K., 1981.

Table 1. Summary of X-ray Crystallographic Data

	3	**4**·0.75CH_2Cl_2·H_2O
formula	$C_{98}H_{82}Fe_2N_2O_{10}$	$C_{98.75}H_{83}Cl_{1.50}Fe_2N_2O_{11}$
fw	1559.36	1638.55
space group	$P2_1/c$	$P\bar{1}$
a, Å	10.9337(9)	16.152(2)
b, Å	24.234(2)	16.874(2)
c, Å	15.1864(13)	17.106(2)
α, deg		109.585(2)
β, deg	107.687(2)	90.022(2)
γ, deg		93.587(2)
V, Å^3	3833.7(6)	4382.5(10)
Z	2	2
ρ_{calc}, g cm^{-3}	1.351	1.242
T, °C	−100	−100
μ(Mo Kα), mm^{-1}	0.445	0.437
θ limits, deg	2.58−25.00	2.42−25.00
total no. of data	52531	60777
no. of unique data	6737	15373
no. of param	505	1060
GOF[a]	1.153	1.046
R^b	0.0757	0.1030
$wR^{2\,c}$	0.1465	0.2395
max, min peaks, e Å^{-3}	0.876, −0.689	1.185, −0.681

[a] GOF (goodness of fit on F^2) = $\{\sum[w(F_o^2 - F_c^2)^2]/(m - n)\}^{1/2}$ (m = number of reflections, n = number of parameters refined). [b] $R = \sum||F_o|-|F_c||/\sum|F_o|$; [c] $wR^2 = \{\sum[w(F_o^2\text{-}F_c^2)^2]/\sum[w(F_o^2)^2]\}^{1/2}$.

protocols are described elsewhere.[21] The structures were solved by direct methods and refined on F^2 with the *SHELXTL* software package.[22] Empirical absorption corrections were applied with *SADABS*,[23] and the structures were checked for higher symmetry using *PLATON*.[24] All non-hydrogen atoms were refined anisotropically. Hydrogen atoms were assigned idealized positions and given thermal parameters equivalent to either 1.5 (methyl hydrogen atoms) or 1.2 (all other hydrogen atoms) times the thermal parameter of the carbon atom to which they are attached. The lattice solvent molecules in the structure of **4** were assigned as partially occupied CH_2Cl_2 (0.5 and 0.25 occupancy, respectively) and water (2 × 0.5 occupancy). The half-occupied CH_2Cl_2 was refined anisotropically. Further attempts to model the disordered solvent molecules in the lattice of **4** were able to lower the *R* factor to 0.0975, but because some of the bond lengths in the resulting model were chemically unreasonable, we elected not to present that alternative. The crystallographic parameters are supplied in Table 1, and selected bond lengths and angles are listed in Table 2.

Table 2. Selected Bond Lengths (Å) and Bond Angles (deg)

		3	
Fe1−O1	2.025(3)	O2−Fe1−O1	123.62(12)
Fe1−O2	1.965(3)	O2−Fe1−O4	117.57(13)
Fe1−O3	2.359(3)	O1−Fe1−O4	117.56(12)
Fe1−O4	2.048(3)	O2−Fe1−N1	94.79(12)
Fe1−N1	2.137(3)	O1−Fe1−N1	91.37(12)
Fe1−Fe1A	4.036	O4−Fe1−N1	95.08(13)
		O2−Fe1−O3	109.91(11)
		O1−Fe1−O3	88.94(11)
		O4−Fe1−O3	58.76(11)
		N1−Fe1−O3	149.97(12)
		4·0.75CH_2Cl_2·H_2O	
Fe1−O2	2.021(4)	O2−Fe1−O6	158.16(18)
Fe1−O4	2.141(5)	O2−Fe1−N2	101.0(2)
Fe1−O6	2.019(4)	O6−Fe1−N2	100.8(2)
Fe1−O8	2.158(5)	O2−Fe1−O4	87.21(18)
Fe1−N2	2.086(5)	O6−Fe1−O4	90.56(18)
Fe2−O1	2.161(5)	N2−Fe1−O4	96.6(2)
Fe2−O3	2.015(4)	O2−Fe1−O8	90.86(17)
Fe2−O5	2.135(4)	O6−Fe1−O8	86.83(18)
Fe2−O7	2.014(4)	N2−Fe1−O8	95.4(2)
Fe2−N1	2.080(6)	O4−Fe1−O8	167.99(18)
Fe1−Fe2	2.778 (1)	O2−Fe1−Fe2	79.16(13)
		O6−Fe1−Fe2	79.00(13)
		N2−Fe1−Fe2	179.27(18)
		O4−Fe1−Fe2	84.14(13)
		O8−Fe1−Fe2	83.85(13)
		O3−Fe2−O7	157.36(19)
		O3−Fe2−N1	100.0(2)
		O7−Fe2−N1	102.6(2)
		O3−Fe2−O5	89.74(18)
		O7−Fe2−O5	87.89(18)
		N1−Fe2−O5	98.7(2)
		O3−Fe2−O1	86.84(17)
		O7−Fe2−O1	90.55(18)
		N1−Fe2−O1	93.9(2)
		O5−Fe2−O1	167.27(18)
		O3−Fe2−Fe1	78.25(13)
		O7−Fe2−Fe1	79.11(14)
		N1−Fe2−Fe1	177.10(18)
		O5−Fe2−Fe1	83.61(13)
		O1−Fe2−Fe1	83.68(13)

Results and Discussion

Synthesis and Crystal Structures of 3 and 4. Although low-spin iron(II) complexes are usually colored,[25,26] high-spin carboxylate-rich diiron(II) compounds are typically colorless or at best yellow,[27−30] making it difficult to analyze their chemistry by standard UV−vis spectroscopic methods. We successfully obtained a chromophoric probe for high-spin diiron(II) compounds in this class by use of 4-CNPy as the nitrogen-donor ligand.[16] This choice was inspired by the hypothesis that a charge-transfer transition from iron(II) to a π^* orbital of the pyridine ligand (MLCT) contributes a shoulder at 370 nm (ϵ = 1400 M^{-1} cm^{-1}) in the optical spectrum of $[Fe_2(\mu\text{-}O_2CAr^{Tol})_4(4\text{-}^t\text{BuPy})_2]$.[17,31] Upon replacement of 4-*tert*-butylpyridine with 4-CNPy, the energy of the acceptor orbital was lowered, thereby reducing the energy gap between the states involved in this transition. This substitution led to a MLCT band in the product that shifted to 510 nm, as anticipated.[16] Acetyl, which has a substituent constant of 0.47, is an electron-withdrawing group like cyano, the substituent constant of which is 0.70.[32] Therefore, a visible absorption band was anticipated for diiron(II) compounds with this alternative nitrogen donor as well.

The syntheses of **3** and **4** followed standard procedures for preparing diiron(II) complexes with 2,6-di-*p*-tolylbenzoate

(21) Kuzelka, J.; Mukhopadhyay, S.; Spingler, B.; Lippard, S. J. *Inorg. Chem.* **2004**, *43*, 1751−1761.
(22) *SHELXTL: Program Library for Structure Solution and Molecular Graphics*, version 6.2; Bruker AXS: Madison, WI, 2002.
(23) Sheldrick, G. M. *SADABS: Area-Detector Absorption Correction*; University of Göttingen: Göttingen, Germany, 2001.
(24) Spek, A. L. *PLATON, A Multipurpose Crystallographic Tool*; Utrecht University: Utrecht, The Netherlands, 2000.
(25) Monat, J. E.; McCusker, J. K. *J. Am. Chem. Soc.* **2000**, *122*, 4092−4097.
(26) Roelfes, G.; Vrajmasu, V.; Chen, K.; Ho, R. Y. N.; Rohde, J.-U.; Zondervan, C.; la Crois, R. M.; Schudde, E. P.; Lutz, M.; Spek, A. L.; Hage, R.; Feringa, B. L.; Münck, E.; Que, L., Jr. *Inorg. Chem.* **2003**, *42*, 2639−2653.
(27) Lee, D.; Pierce, B.; Krebs, C.; Hendrich, M. P.; Huynh, B. H.; Lippard, S. J. *J. Am. Chem. Soc.* **2002**, *124*, 3993−4007.
(28) Lee, D.; Lippard, S. J. *Inorg. Chim. Acta* **2002**, *341*, 1−11.
(29) Lee, D.; DuBois, J. L.; Pierce, B.; Hedman, B.; Hodgson, K. O.; Hendrich, M. P.; Lippard, S. J. *Inorg. Chem.* **2002**, *41*, 3172−3182.
(30) Lee, D.; Lippard, S. J. *Inorg. Chem.* **2002**, *41*, 827−837.
(31) Lee, D.; Du Bois, J.; Petasis, D.; Hendrich, M. P.; Krebs, C.; Huynh, B. H.; Lippard, S. J. *J. Am. Chem.* Soc. **1999**, *121*, 9893−9894.
(32) Carey, F. A.; Sundberg, R. J. *Advanced Organic Chemistry*, 3rd ed.; Plenum Press: New York, 1990.

Scheme 1

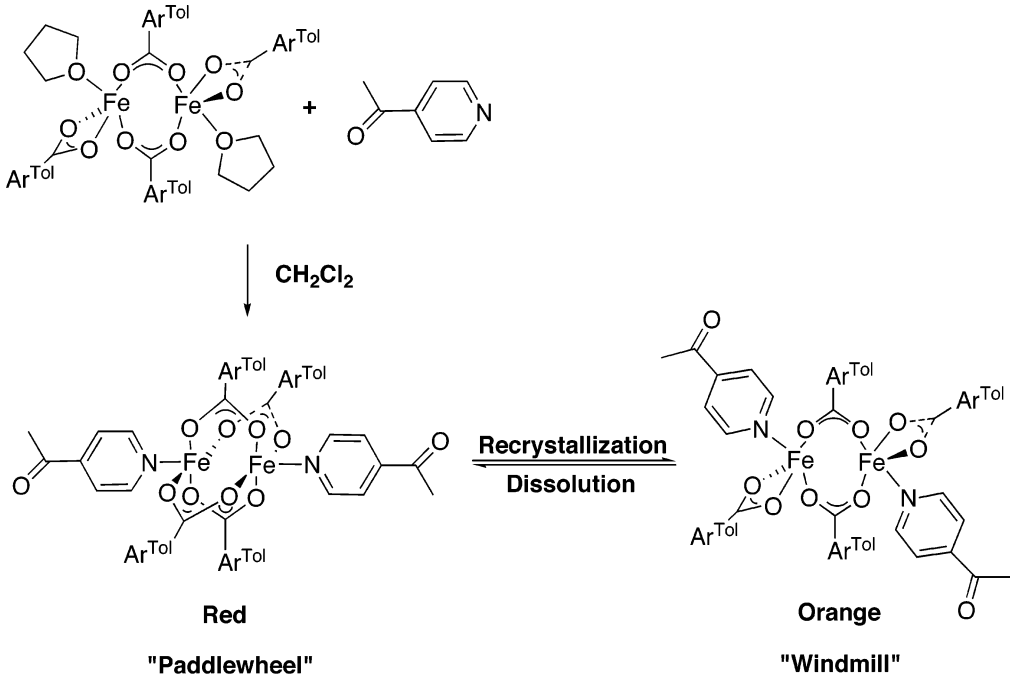

ligands.[33] Upon the addition of neat 4-AcPy to a yellow CH_2Cl_2 solution of $[Fe_2(\mu\text{-}O_2CAr^{Tol})_2(O_2CAr^{Tol})_2(THF)_2]$, a red color developed immediately (Scheme 1). After pentane vapor diffusion, needles of **3** formed that were orange instead of red. These needles were quite stable in Paratone-N oil, and no fissures were observed after 1 day. X-ray analysis revealed the windmill structure depicted in Figure 1. Two crystallographically equivalent iron atoms, bridged by two carboxylates, are related by an inversion center at a distance of 4.036 Å. Both iron atoms adopt a highly distorted trigonal-bipyramidal coordination geometry, with ligand donor atoms supplied by two bridging carboxylates, a bidentate carboxylate, and a 4-AcPy molecule.

When compound **3** was dissolved in CH_2Cl_2, a red homogeneous solution with λ_{max} at 495 nm ($\epsilon = 1300\ M^{-1}\ cm^{-1}$) gradually formed. Rapid removal of the solvent afforded a red powder. Recrystallization from a concentrated solution by pentane vapor diffusion afforded both orange needles (**3**) and red-orange dichroic plates (**4**). Unlike the former, the latter crystals developed cracks in several minutes after being removed from the mother liquor. In the structure of **4**, there are two crystallographically inequivalent square-pyramidal iron atoms and four bridging carboxylate ligands, which affords a shorter Fe···Fe distance, 2.778(1) Å, between the two iron atoms (Figure 2). The nitrogen atoms of the 4-AcPy ligands coordinate to iron at the apical positions circumscribed by the axial pockets generated by the four bridging carboxylates. Both structures of **3** and **4** are geometrically quite similar to windmill[17,34] or paddlewheel[16,31,35] compounds reported previously.

The interconversion of **3** and **4** is the result of carboxylate shifts, which are well-documented for this type of carboxylate-rich diiron(II) complex.[17] However, the present example is the first in which the two structures can be distinguished by their colors. Considering that, in solution, both compounds adopt a paddlewheel structure and that both **1** (see below) and $[Fe_2(\mu\text{-}O_2CAr^{4-FPh})_4(4\text{-}^tBuPy)_2]$[17] retain a paddlewheel

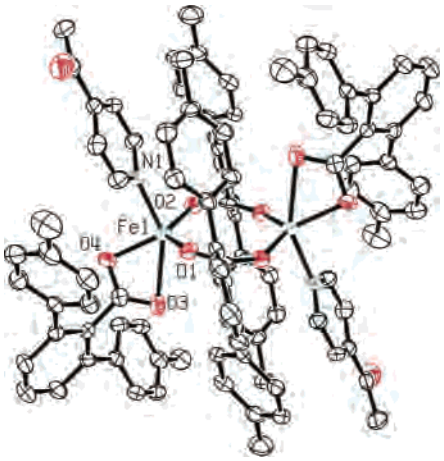

Figure 1. ORTEP diagram of **3** (50% probability thermal ellipsoids) depicting all non-hydrogen atoms.

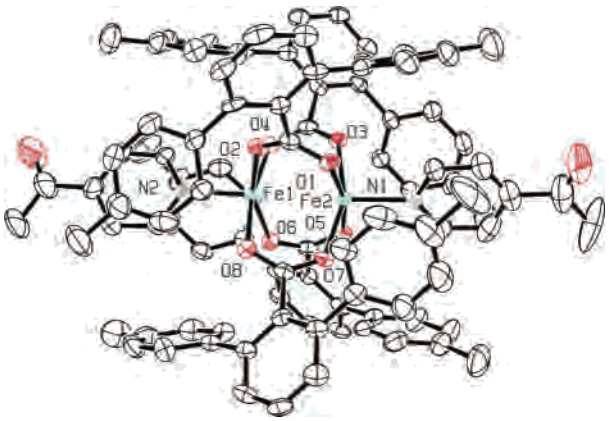

Figure 2. ORTEP diagram of **4** (50% probability thermal ellipsoids) showing non-hydrogen atoms.

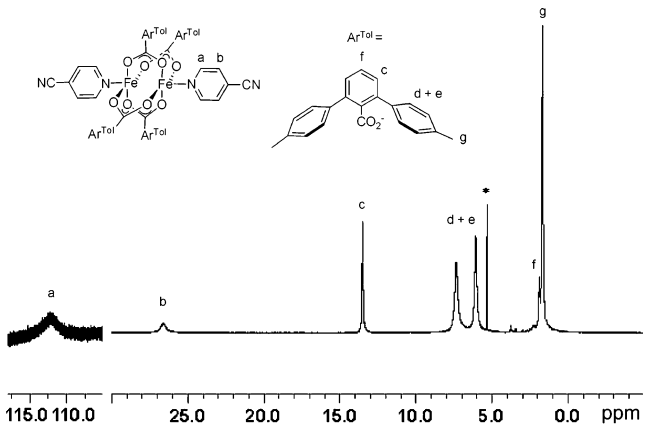

Figure 3. NMR spectrum of **1** in CD_2Cl_2 at 20 °C. The solvent peak is marked with an asterisk.

structure in solution over the temperature range of 203−293 K, we propose the following guideline. A sterically hindered, carboxylate-rich diiron(II) compound, with a para-substituted pyridine as the nitrogen donor, will adopt a paddlewheel structure in a strictly anhydrous solution unless an ancillary ligand such as water coordinates to the molecule and converts the complex to a windmill structure. Further work is required to test the generality of this proposal.

^{1}H NMR Spectral Studies. At room temperature, seven resolved signals appear in the 0−160 ppm region of the ^{1}H NMR spectrum of **1** (Figure 3). No additional peaks of significance occur in the variable-temperature 1D spectra (Figure S1 in the Supporting Information) recorded in the interval 293−203 K, suggesting that **1** retains the paddlewheel structure in this temperature range. The presence of seven resonances implies that there is an additional (pseudo)-symmetry plane present in the molecule besides the C_2 axis observed in the crystal structure. Thus, the four bridging carboxylate and two 4-CNPy ligands each give rise to only one set of NMR resonances. In general, protons in close proximity to the iron atoms will be more significantly affected by their paramagnetism and therefore have broader line widths arising from shorter transverse relaxation times (T2). We therefore assign the broadest peak (resonance a) at low field (112 ppm at 293 K) in the spectrum to hydrogen atoms in the 2 and 6 positions of 4-CNPy because they are closest to iron, with an average H−Fe distance of 3.029 Å. The relative intensities of the lines were measured at 203 K when the signals appear sharpest. Resonances b and f integrate as 1:1, with the former broader than the latter at room temperature. Accordingly, resonance b is assigned to protons in the 3 and 5 positions of 4-CNPy and resonance f is assigned to the proton at the 4 position of the benzoate group, because the former is closer to the iron atoms. The average H−Fe distance for the former is about 5.0 Å, whereas for the latter, it is >7.9 Å. These assignments are consistent with those in related high-spin iron(II) compounds.[36] The remaining peaks are assigned to benzoate ligand protons based on their relative intensities. Signals d and e are assigned to the ring protons of the tolyl group, which cannot be distinguished from one another. The 2D COSY ^{1}H NMR spectrum at 273 K gave a cross peak only between resonances c and f, which we assign to the para and meta protons of the benzoate group; they are relatively removed from the paramagnetic center and display sharper signals than other protons. The ^{1}H NMR spectrum of **4** is similar to that of **1**, as expected for a paddlewheel complex, with the resonance of the acetyl methyl group occurring at 2.5 ppm.

At room temperature, the solution NMR spectrum of **2** is almost identical with that of the anhydrous compound, **1**, consistent with loss of water molecules when **2** dissolves in solution. In a related system, the equilibrium in eq 1 was proposed, with $\Delta H = -95(11)$ kJ mol^{-1} and $\Delta S = -253(47)$

$$\mathbf{1} + 2H_2O \rightleftharpoons \mathbf{2} \qquad (1)$$

J mol^{-1} K^{-1}.[16] Because water binding is favorable at low temperature, we would expect new signals to appear, corresponding to the postulated structural change, whereas the signals of **1** disappear as the temperature is lowered. However, when comparing the variable-temperature 1D NMR spectrum of **2** (Figure S2 in the Supporting Information) with that of **1**, we note that the major signal changes are identical and appear to arise from the anhydrous compound, with several broad and small signals (44, 16, 15, and 14 ppm at 253 K) appearing below 273 K. The persistence of the peaks in a D_2O sample indicates that these resonances cannot be ascribed to water molecules bound to the iron atoms, although their proton signal would be expected to be too broad to be observed owing to their proximity to the paramagnetic center. We can therefore assign these resonances to other protons in the water adduct. The reason the changes are not significant is because the solubility of water in CH_2Cl_2 changes dramatically with temperature. The solution prepared at room temperature has a concentration of around 7 mM. It has been reported that water separates from a CH_2Cl_2 solution as a clathrate ($CH_2Cl_2 \cdot 34H_2O$) below −0.8 °C[37] and that water solutions with concentrations >2 mM in CH_2Cl_2 form a clathrate at −40 °C or below.[38] At low temperature, the amount of free water molecules decreases dramatically because of the formation of clathrate and therefore shifts the equilibrium shown in eq 1 to the left, resulting in a predominance of the anhydrous compound **1** and weak signals from the water-bound diiron compound **2**.

An experiment was then designed in which excess water (13 equiv) was added to a CD_2Cl_2 solution of **1**. After filtration, the NMR spectrum of the filtrate (Figure S3 in the Supporting Information), which corresponds to that of the water adduct, was recorded. No effort was made to assign

(33) Lee, D.; Lippard, S. J. In *Comprehensive Coordination Chemistry II*; McCleverty, J. A., Meyer, T. J., Eds.; Elsevier Ltd.: Oxford, U.K., 2004; Vol. 8, pp 309−342.
(34) Lee, D.; Lippard, S. J. *J. Am. Chem. Soc.* **1998**, *120*, 12153−12154.
(35) Yoon, S.; Lippard, S. J. *Inorg. Chem.* **2003**, *42*, 8606−8608.
(36) Hagadorn, J. R.; Que, L., Jr.; Tolman, W. B. *Inorg. Chem.* **2000**, *39*, 6086−6090.
(37) Kaloustian, J.; Rosso, J. C.; Caranoni, C.; Carbonnel, L. *Rev. Chim. Miner.* **1976**, *13*, 334−342.
(38) Kryatov, S. V.; Rybak-Akimova, E. V.; MacMurdo, V. L.; Que, L., Jr. *Inorg. Chem.* **2001**, *40*, 2220−2228.

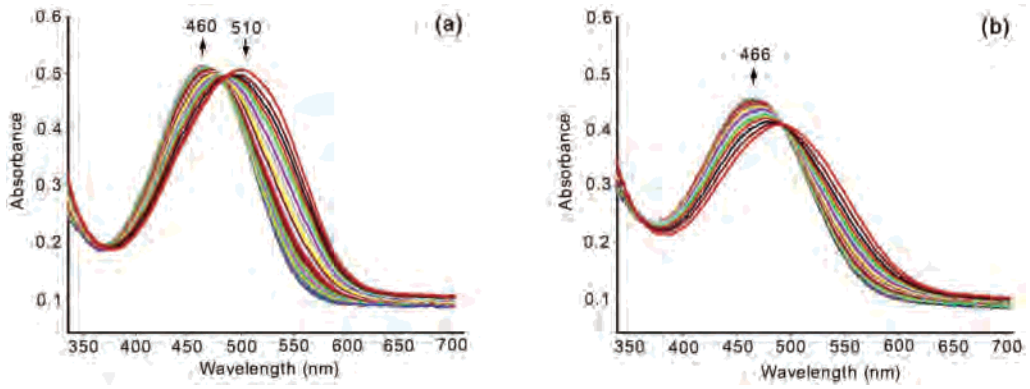

Figure 4. UV−vis spectral changes as a function of time when **1** (a) and **4** (b) reacted with water in CH_2Cl_2 at 198 K. (a) A total of 200 scans were collected at equal intervals over 7 s. (b) A total of 300 scans were collected at equal intervals over 1.5 s.

the signals because of the complexity of the spectrum, but a very broad peak was observed around 46 ppm, which may arise from protons in the 2 and 6 positions of the pyridine rings in a windmill structure. This resonance corresponds to the new signal detected in the variable-temperature spectra of **2**, indicating formation of an aqua adduct at lower temperature.

To summarize, NMR spectroscopy affords some information about the formation and nature of an aqua complex, but this method is limited by water solubility in CH_2Cl_2 solutions at low temperature.

Effect of Water on the Oxygenation of 1 and 4. Competition between dioxygen and water for **1** was investigated between 198 and 293 K by using stopped-flow spectroscopy.[16] Aquation of **1** was concluded previously to occur at least 1000 times faster than oxygenation of **1**.[16] This estimate was refined here by studying directly the reaction of compound **1** with water and of the resultant aqua compound **2** with dioxygen.

(a) Reaction with Water. In the present study, the kinetics of the aquation of **1** were measured between 198 and 223 K. To ensure pseudo-first-order conditions, the initial concentrations of **1** and water in CH_2Cl_2 were 0.177 and 1 mM, respectively. A distinctive shift in the absorbance maximum from 510 to 460 nm occurred (Figure 4), with the former arising from the anhydrous compound **1** and the latter from the water adduct **2**. The change in the intensity at 510 nm versus time was fit to eq 2 by a nonlinear least-squares procedure, where A_∞ and A_0 are the optical absor-

$$A_t = A_\infty - (A_\infty - A_0)\exp(-k_{obs}t) \qquad (2)$$

bances at infinity and zero times, respectively. Our observed rate constants, k_{obs1}(**1**) (Table 3), are comparable to those obtained in a competition experiment [k_{obs}(aquation) in Table 4],[16] indicating that only aquation occurs on this time scale.

This reaction was further investigated at −60 °C with different excess amounts of water. A plot of ln k_{obs1}(**1**) vs ln [H_2O] was fitted to a linear equation, which had a slope of 0.99(4) (Figure 5a), indicating a first-order dependence on water. The pseudo-first-order rate constant is also linearly dependent on the concentration of water (Figure 5b), with an intercept, which corresponds to the reverse reaction rate constant, near zero. This result indicates the reaction to be

Table 3. Pseudo-First-Order Rate Constants (s^{-1}) Obtained for Aquation (k_{obs1}), Oxygenation under Anhydrous Conditions (k_{obs2}), and Oxygenation of the Aquated Forms (k_{obs3}) of **1** and **4**[a]

T (°C)	k_{obs1}(**1**)	k_{obs1}(**4**)	T (°C)	k_{obs2}(**1**)[b]	k_{obs2}(**4**)	k_{obs3}(**1**)	k_{obs3}(**4**)
−75	1.69(5)	8.01(4)	−40			0.192(3)	0.106(1)
−70	4.17(3)	15.2(3)	−30	0.045(5)		0.469(4)	0.324(6)
−65	9.0(1)	24.4(7)	−20	0.10(1)	0.0429(4)	1.10(1)	0.891(7)
−60	18.2(3)	42.5(4)	−10	0.20(1)	0.101(5)	2.66(4)	2.12(1)
−55	39.8(8)	72.5(9)	0	0.40(2)	0.206(8)	6.13(3)	4.47(8)
−50	82.2(6)		10	0.71(6)	0.446(8)	12.0(2)	8.48(13)
			20	1.4(3)	0.973(46)	20.3(5)	16.1(4)

[a] Details are given in the text. [b] Reference 16.

Table 4. Rate Constants (s^{-1}) from a Competition Experiment in Which the Kinetic Rate Constants for the Reaction of **1** with Dioxygen versus Water Were Measured in a Dioxygen/Water-Containing CH_2Cl_2 Solution[a]

T (°C)	k_{obs}(aquation)	T (°C)	k_{obs}(oxygenation)
−75	2.5(1)	−40	0.12(1)
−70	5.1(2)	−30	0.39(12)
−65	11.1(8)	−20	1.21(17)
−60	23.7(17)	−10	2.7(2)
−55	43.0(24)	0	5.5(5)
−50	62.8(5)	10	9.1(10)
		20	14.6(7)

[a] Details are provided in ref 16.

irreversible under these conditions. Taken together, the data reveal that the reaction of water with **1** follows a rate law that can be described by eq 3, with $k = 18.2\ M^{-1}\ s^{-1}$.

$$-d[\mathbf{1}]/dt = k[\mathbf{1}][H_2O] \qquad (3)$$

Compound **4** has an absorbance maximum at 495 nm, and its reaction with water generates a species that absorbs at 466 nm, like compound **3** (Figure 4). This process was also studied kinetically from −75 to −50 °C in a single-mixing stopped-flow experiment. The addition of excess water (1.0 mM in CH_2Cl_2) to **4** (0.160 mM in CH_2Cl_2) increased the intensity at 466 nm, and the kinetics were fit to a pseudo-first-order reaction. The rate constants k_{obs1}(**4**) are listed in Table 3. An attempt was made to determine the order in water for the aquation of **4** at −70 °C. At a concentration of **4** of 0.062 mM used in this experiment, reaction with water afforded an absorbance intensity change at 466 nm of less than 0.01. The accuracy of the rate constants derived from the data was therefore low, and no firm conclusion could be

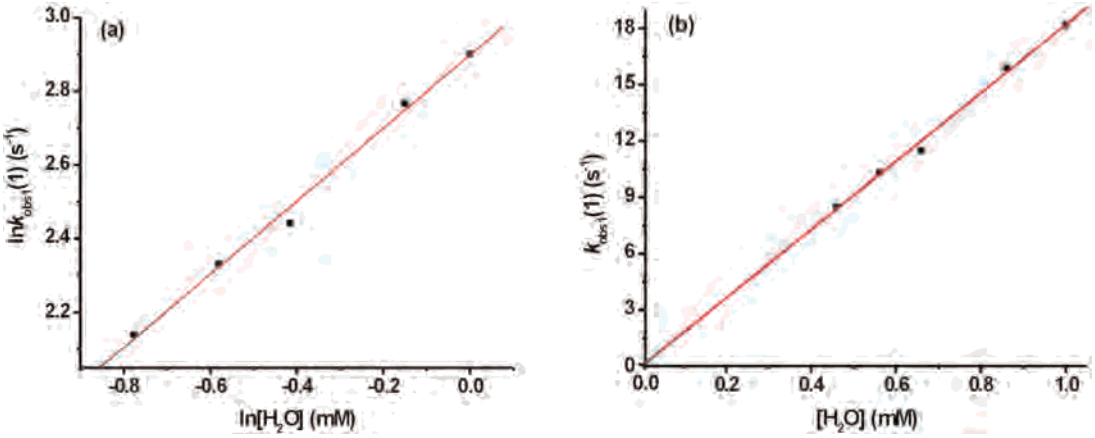

Figure 5. Plot of ln k_{obs1}(**1**) vs ln [H_2O] (a) and plot of k_{obs1}(**1**) vs [H_2O] (b). The measurements were conducted at −60 °C, with [**1**] = 0.0585 mM in CH_2Cl_2.

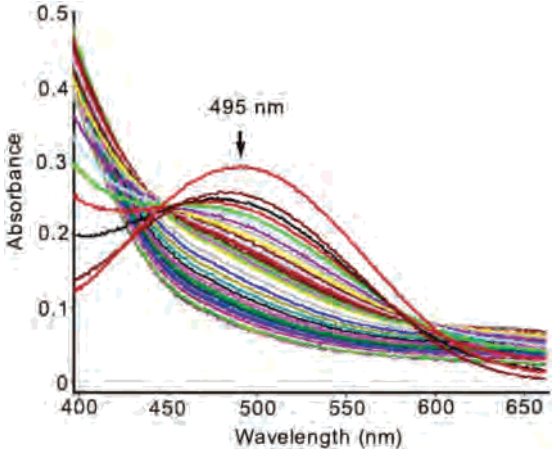

Figure 6. UV−vis spectral change when **4** reacts with anhydrous dioxygen at 253 K. A total of 300 scans were collected at equal intervals over 105 s.

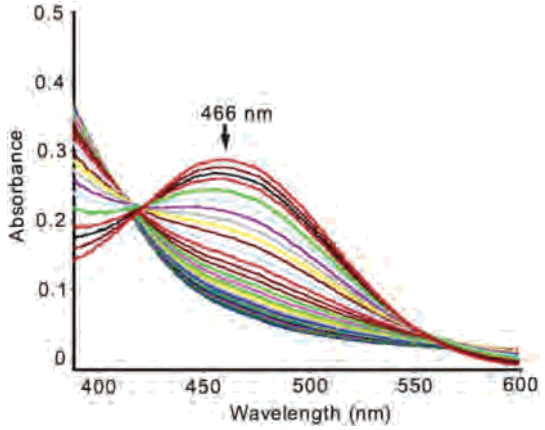

Figure 7. UV−vis spectral change as a function of time in the double-mixing experiment: **4** reacted with water in the first mixer and subsequently reacted with dioxygen. A total of 200 scans were collected at equal intervals over 100 s.

drawn about the order of the reaction in water. Although the structure of the water adduct of **4** has not been determined, a titration experiment indicated a 1:2 ratio for **4**/water, suggesting the formation of a diaqua complex, probably quite similar to compound **2**.

(b) Reaction with Dioxygen in an Anhydrous Solution. The oxygenation of **1** in an anhydrous environment has been studied in detail [k_{obs2}(**1**), Table 3].[16] The reactivity of **4** with dioxygen was similarly examined between −20 and +20 °C. Upon mixing with dioxygen, the distinctive 495-nm absorbance began to decrease (Figure 6), generating a yellow solution. Failure to maintain an isosbestic point as the reaction progresses indicates that the initially formed product undergoes a further transformation. The kinetic traces were fit to an expression for first-order decay, and pseudo-first-order rate constants k_{obs2}(**4**) were obtained. From the temperature dependence of these rate constants (Table 3), we calculated the activation parameters: $\Delta H^{\ddagger} = 45(2)$ kJ mol^{-1} and $\Delta S^{\ddagger} = -92.0(7)$ J mol^{-1} K^{-1} (Figure S4 in the Supporting Information).

(c) Double-Mixing Experiments. After **1** was mixed with water, the solution was further allowed to react with excess dioxygen in a second push using the double-mixing stopped-flow apparatus. Experiments were conducted in the temperature range from 233 to 293 K. The 460-nm absorbance arising from the aqua adduct decreased with time, a change that could be nicely fit to a pseudo-first-order expression. The derived rate constants k_{obs3}(**1**) are comparable to those obtained from a previous competition experiment [k_{obs}(oxygenation) in Table 4],[16] which indicates that aquation was completed prior to oxygenation.

A similar behavior was observed for **4**. An absorbance at 466 nm, indicative of the windmill structure, began to decrease upon mixing with dioxygen (Figure 7). The derived rate constants k_{obs3}(**4**) are listed in Table 3. When k_{obs3} is compared with k_{obs2}, it can be concluded that water reacts with the diiron(II) compounds more rapidly than dioxygen and accelerates the oxygenation of diiron(II) complexes. Oxygenation of **4** is 20-fold faster when water is present than in its absence, and the reactivity of **1** similarly improves by 10-fold under such conditions. From the temperature dependence of k_{obs3}(**4**), we derived the following activation parameters: $\Delta H^{\ddagger} = 45(2)$ kJ mol^{-1} and $\Delta S^{\ddagger} = -61.8(7)$ J mol^{-1} K^{-1} (Figure S5 in the Supporting Information). A comparison of these values with those from the anhydrous oxygenation study reveals similar enthalpies of activation, indicating that the transition state most likely does not involve loss of water prior to dioxygen attack. Instead, we propose

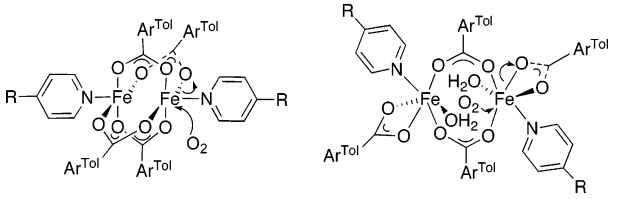

Figure 8. Proposed transition states for the dioxygen reaction.

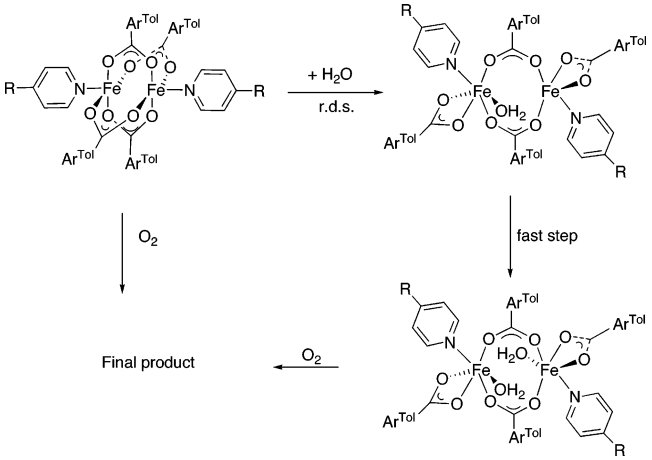

Figure 9. Generalized mechanism for oxygenation with or without the presence of water.

the cleavage of one carboxylate−iron bond to provide a site for attack by the dioxygen molecule. To satisfy the coordination requirements of the iron atom, the Fe−O bond might be partially broken in the transition state involving the paddlewheel structure in anhydrous CH_2Cl_2, whereas the Fe−O bond in the aquated windmill structure might be cleaved completely. This difference would explain the less negative entropy in the latter case (Figure 8).

(d) Mechanistic Considerations. We previously proposed a mechanism for the oxygenation of **1**[16] involving the diaqua adduct **2** as the product of aquation, based on a single-mixing kinetic study. From the present data, we proposed a slightly modified version (Figure 9), which may apply more generally to structurally related compounds in this class. In an environment where there is an excess of both water and dioxygen, the paddlewheel compound reacts with a molecule of water and converts it to the windmill structure. In the presence of excess water, this rate-determining step is followed by a very fast process, in which a second water molecule binds to the diiron center to produce a diaqua species. This compound then reacts with dioxygen to give the final product. One reason for the faster oxygenation rates in the aqueous environment is the change in geometry. In the paddlewheel structure, the diiron center is significantly shielded by the four carboxlate ligands. Its square-pyramidal geometry makes it nearly impossible for dioxygen to attack an iron atom from a position trans to the nitrogen donor, and attack from the same side, as depicted in Figure 8, is retarded by steric factors. In a windmill structure, with two bridging ligands instead of four and the Fe−Fe distance elongated, the iron atoms are more accessible to attack by dioxygen. Also, water molecules provide a proton source for the oxygenated intermediate to convert to a $(\mu\text{-OH})_2Fe^{III}_2$ species, which is typically encountered in the final products. This hydrogen-bonding feature could contribute to the rate acceleration.

Conclusion

We prepared two isomeric compounds with 4-AcPy ligands that can be distinguished by their color, the first pair of complexes having this property. Both paddlewheel and windmill structures are present in the solid state, whereas only the paddlewheel form exists in an anhydrous CH_2Cl_2 solution. Water can induce conversion to a windmill structure in solution, the details of which were investigated by stopped-flow kinetic experiments. It was determined that the aquation is first-order in both the diiron complex and water. Water reacts with diiron complexes much faster than dioxygen, and the reactivity with dioxygen is significantly increased when water is present.

Acknowledgment. This work was supported by Grant GM-32134 from the National Institute of General Medical Sciences. We thank Drs. Sungho Yoon and Dong Xu for helpful discussions.

Supporting Information Available: X-ray crystallographic information (CIF files) for **3** and **4**; Figures S1 and S2 showing variable-temperature NMR spectra of **1** and **2**; Figure S3 displaying the NMR of the reaction mixture from **1** and excess water; and Figures S4 and S5 showing the Eyring plots of k_{obs2}(**4**) and k_{obs3}(**4**). This material is available free of charge via the Internet at http://pubs.acs.org.

IC0602906